CHAPTER NINE

Electrocatalytic Oxidation of Diethylaminoethanethiol, Hydrazine and Nitrite at Single-Walled Carbon Nanotubes Modified with Prussian Blue Nanoparticles*

* The publication below resulted from part of the research work presented in this chapter and it is not referenced further in this thesis:

10. **Abolanle S. Adekunle**, Kenneth I. Ozoemena, *Electroanalysis* DOI:10.1002/élan.201000289 (in press).

9.1 Microscopic and spectroscopic characterisation

Figure 9.1 presents the TEM images of PB nanparticles (Figure 9.1a) and SWCNT-PB nanocomposite (Figure 9.1b). From the TEM pictures, the PB particles appeared porous, amorphous, evenly distributed along the nanotubes and are in the size distribution of 5 – 15 nm.

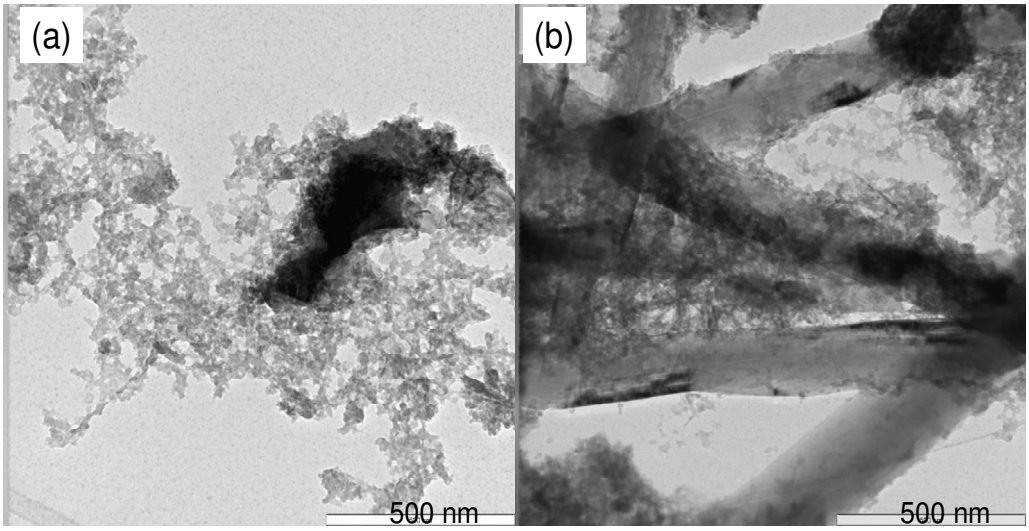

Figure 9.1: TEM of (a) Prussian blue (PB) nanoparticles (b) SWCNT-PB nanocomposite.

The PB particle distribution on the walls of the CNT could be due to both electronic (Covalent bonding) and ionic interaction between the phenyl ring, NH_2 or the SO_3^{2-} groups of the SWCNT-PABS and the PB ($Fe_4(III)[Fe(II)(CN)_6]_3$) nanoparticles. Figure 9.2 is the FTIR of (i) SWCNT-PABS and (ii) SWCNT-PB. The band at around 1026 cm^{-1} could be due to S=O stretching modes of the sulfonic acid group ($-SO_3^{2-}$) of the SWCNT-PABS. The strong band at 1380 cm^{-1} which appeared sharper in (ii) could be due to the N=O of NO_2 formed from the oxidation of NH_2 of the SWCNT-PABS. The band at around 1620

cm^{-1} common to (i) and (ii) is due to the vibration mode of C=C bonds. The bands at 2194, 2082 and 1936 cm^{-1}, found in (ii) but absent in (i) confirms the presence of C=N bond formed by the interaction of PB nanoparticles with the SWCNT-PABS. The band at 2915 and 2847 cm^{-1} common to both spectra can be attributed to C-H stretching bond of the sp^3 hybridised carbon of the SWCNT-PABS. The intense band at 3419 cm^{-1}, common to both spectra is ascribed to the N-H and/or O-H group of adsorbed moisture during sample preparations and was more in (ii) due to its broad band.

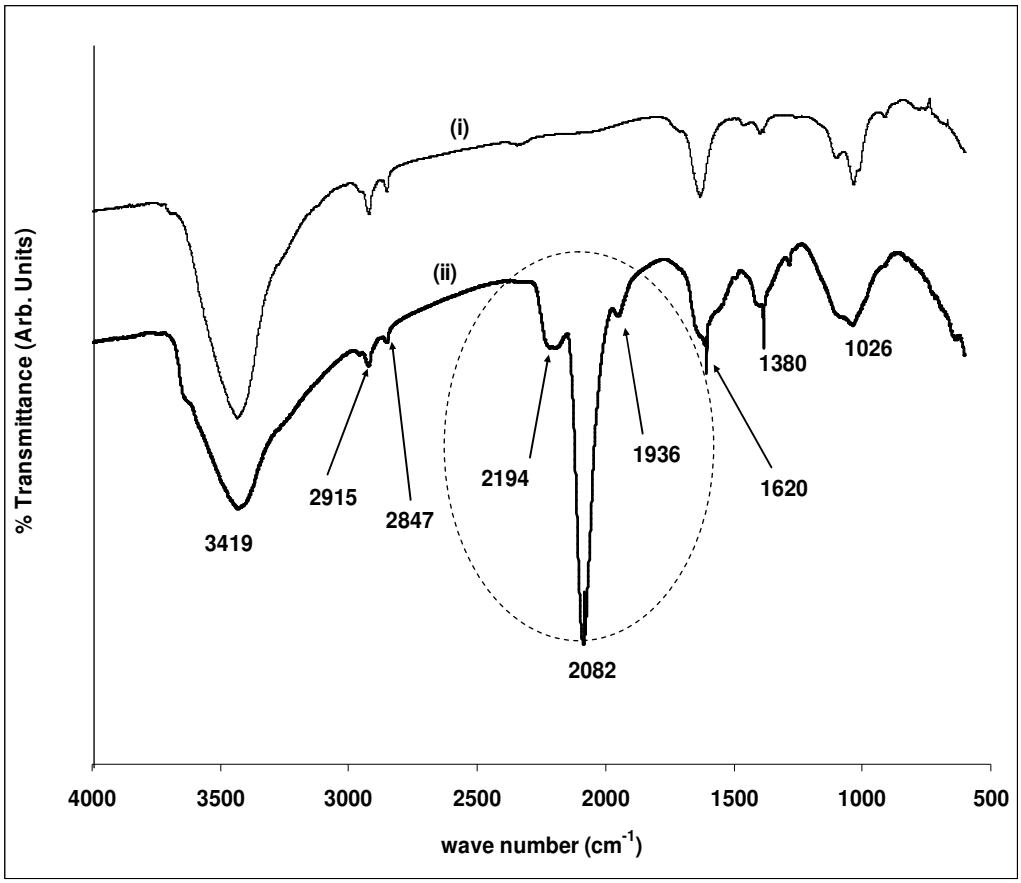

Figure 9.2: FTIR spectra of (i) SWCNT-PABS and (ii) SWCNT-PB nanocomposite.

XPS result (Figure 9.3) shows the two oxidized forms of iron, Fe^{2+} and Fe^{3+}. This is in agreement with the molecular structure of PB ($Fe_4(III)[Fe(II)(CN)_6]_3$) where the Fe occurs in two oxidation states. Inset in Figure 9.3 is the XPS indicating clearly the Fe peaks, and the dominance of Fe^{3+} peak over Fe^{2+} peak. The binding energies for the peaks at 712.5 and 726.0 eV are characteristic doublet from Fe $2p_{3/2}$ and Fe $2p_{1/2}$ [1] and agreed closely with literature values of 711.0 and 724.6 eV associated with the presence of Fe_2O_3 and Fe_3O_4 species respectively [2]. The nitrogen (N) and the carbon (C) peaks of the SWCNT-PABS and PB nanoparticles were seen at 401 and 285.5 eV respectively.

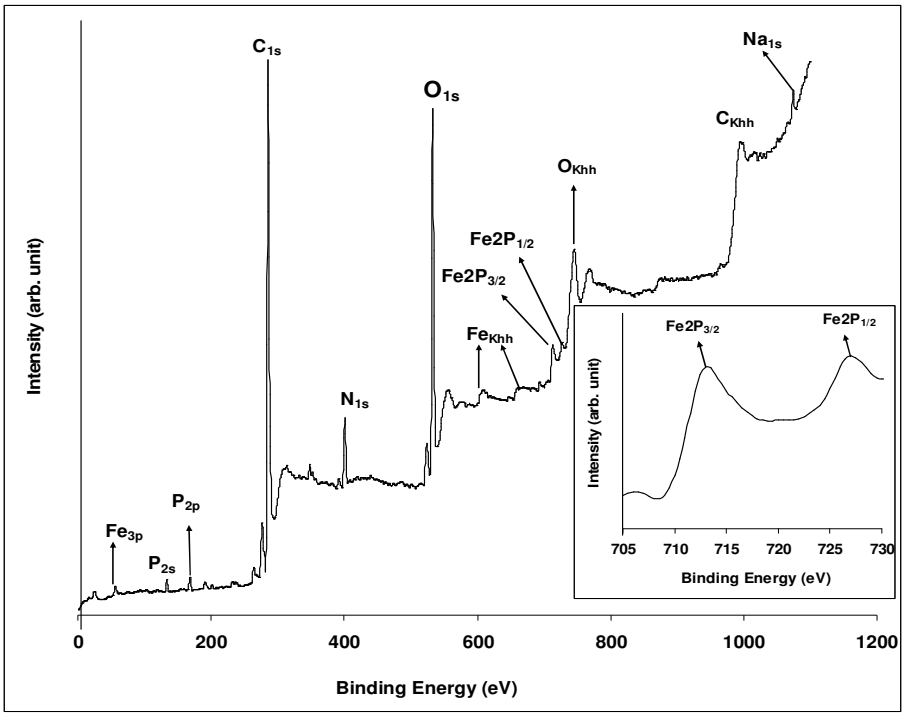

Figure 9.3: XPS spectrum of SWCNT-PB showing the presence of Fe^{2+} and Fe^{3+} ions the PB nanoparticles. Inset is the XPS spectrum indicating clearly the Fe peaks and the dominance of Fe^{3+} peak over Fe^{2+} peak.

Figure 9.4a and 9.4b showed the EDX spectrum of the SWCNT-PABS the SWCNT-PB nanocomposite of bare glassy carbon (GC) plate. GC plate was used as supporting electrode for obtaining the pictures since it is the next available platform (in place of EPPGE) to fit into the equipment. As expected, the EDX of the SWCNT-PABS was predominantly dominated by carbon peaks. The carbon peak was also prominent on the EDX of the SWCNT-PB. The N peak overlaps with the C peak but the elemental results indicates its occurrence in reasonable amount (13%), while the Fe peak was associated with the Fe^{2+} and the Fe^{3+} of the PB nanoparticles thus implying successful transformation of the SWCNT-PABS to SWCNT-PB. The potassium (K) peak is expected from the PB nanoparticles.

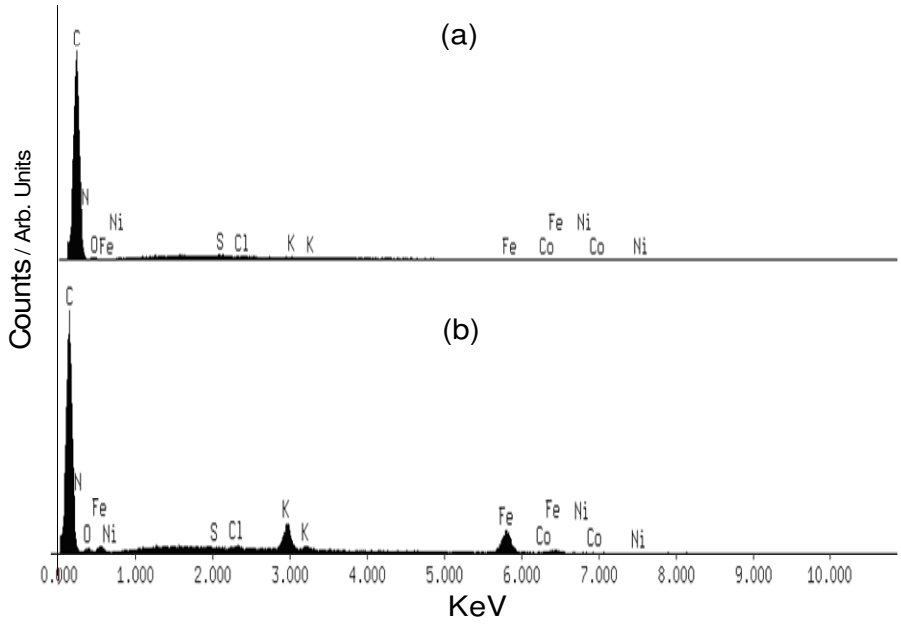

Figure 9.4: EDX spectra of (a) SWCNT-PABS and (b) SWCNT-PB nanocomposites.

9.2 Electrochemical characterization

Figure 9.5 compares the cyclic voltammograms of the bare EPPGE, EPPGE-SWCNT-PABS, EPPGE-PB and EPPGE-SWCNT-PB in PBS (pH 7.0) containing 0.1 M KCl. The CVs gave several properties already described under section 8.2. The signature peaks (PB/PW) were enhanced by the presence of the SWCNT, indicating the enhanced electron-conducting impact of the SWCNTs as redox mediator. The Prussian yellow (PY) is ill-defined at ~ 0.8 V (see Figure 9.5b). These peaks are consistent with literature [3,4]. Note from Figure 9.5b that the SWCNT-PB film showed little change (13% current decrease) when the electrode was subjected to continuous cycling in the electrolyte, a clear indication of excellent electrochemical stability (*ca* 90%). The surface concentration of the PB nanoparticles on the EPPGE-SWCNT-PB platform (Γ_{PB} / mol cm^{-2}) was estimated using a known relationship [5]. The value of the Γ_{PB} was estimated as ~ 4.8 x 10^{-8} mol cm^{-2}. The value is a magnitude higher than 4-5 x 10^{-9} mol cm^{-2} of PB films on glassy carbon (GC) electrode [6] for electrocatalytic reduction of H_2O_2, and agrees favourably with the 1.1 to 2.2 x 10^{-8} mol cm^{-2} of PB concentration on GC for electrocatalytic reduction of molecular oxygen [7].

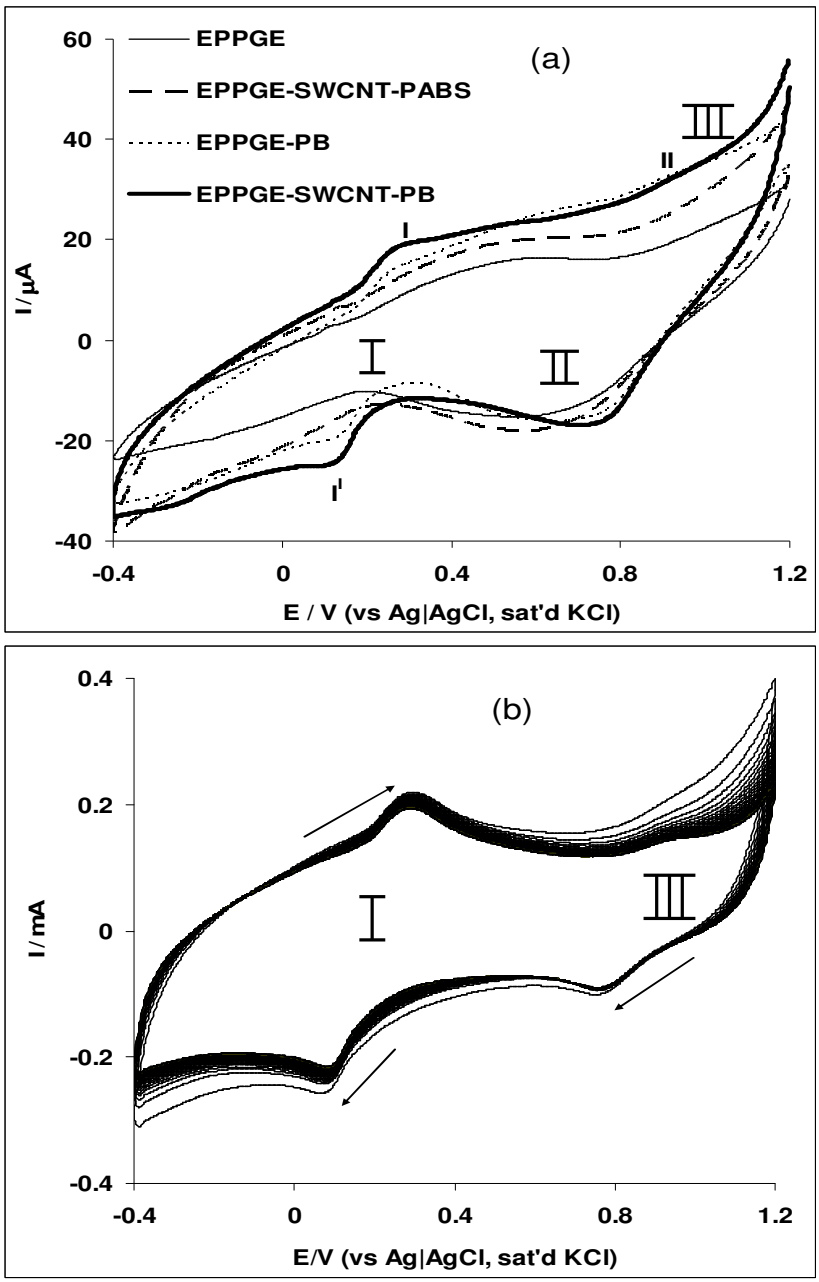

Figure 9.5: (a) Cyclic voltammograms showing the current responses of the electrodes modified with and without 10^{-4} M PB Prussian blue in 0.1 M KCl within the potential range of -0.4 to 1.2 V. Scan rate: 25 mVs^{-1}. (b) Current response of the EPPGE-SWCNT-PB electrode (30 scans) in (a) 0.1 M KCl electrolyte.

9.3 Electrocatalytic oxidation properties

Figure 9.6 presents the comparative background-subtracted voltammetric responses of the four electrodes in the solutions of (a) 0.1 mM DEAET (pH 9.4 PBS), (b) 1 mM hydrazine (0.1 M Na_2SO_4), (c) 10^{-3} M NO_2^- at pH 7.4 PBS and (d) 10^{-3} M NO at pH 3.0 PBS (Scan rate: 25 mVs^{-1}).

Electrocatalytic oxidation of DEAET was carried out in pH 9.4 PBS since previous studies had shown that DEAET gave best response under alkaline pH conditions [8,9]. The voltammetric data, in terms of current response (I_p) and peak potential (E_p) are summarised in Table 9.1. In all cases, the EPPGE-SWCNT-PB gave the best electrochemical response, thus all further studies were concentrated on this electrode.

The stability of the EPPGE-SWCNT-PB electrode towards the detection of these analytes was studied by repetitively cycling the solution of the analyte (30 scans, CV not shown). A decrease in peak current was observed after the first scan, which is typical of a poisoned electrode. However, upon rinsing the electrode in a fresh electrolyte, the electrode surface was renewed with about 84% of the initial catalytic current obtained, suggesting satisfactory electrochemical stability and reusability of the electrode after analysis. The electrode can be used for the analysis of DEAET, hydrazine and nitrite after storage in a refrigerator for up to two weeks without a significant change in its response.

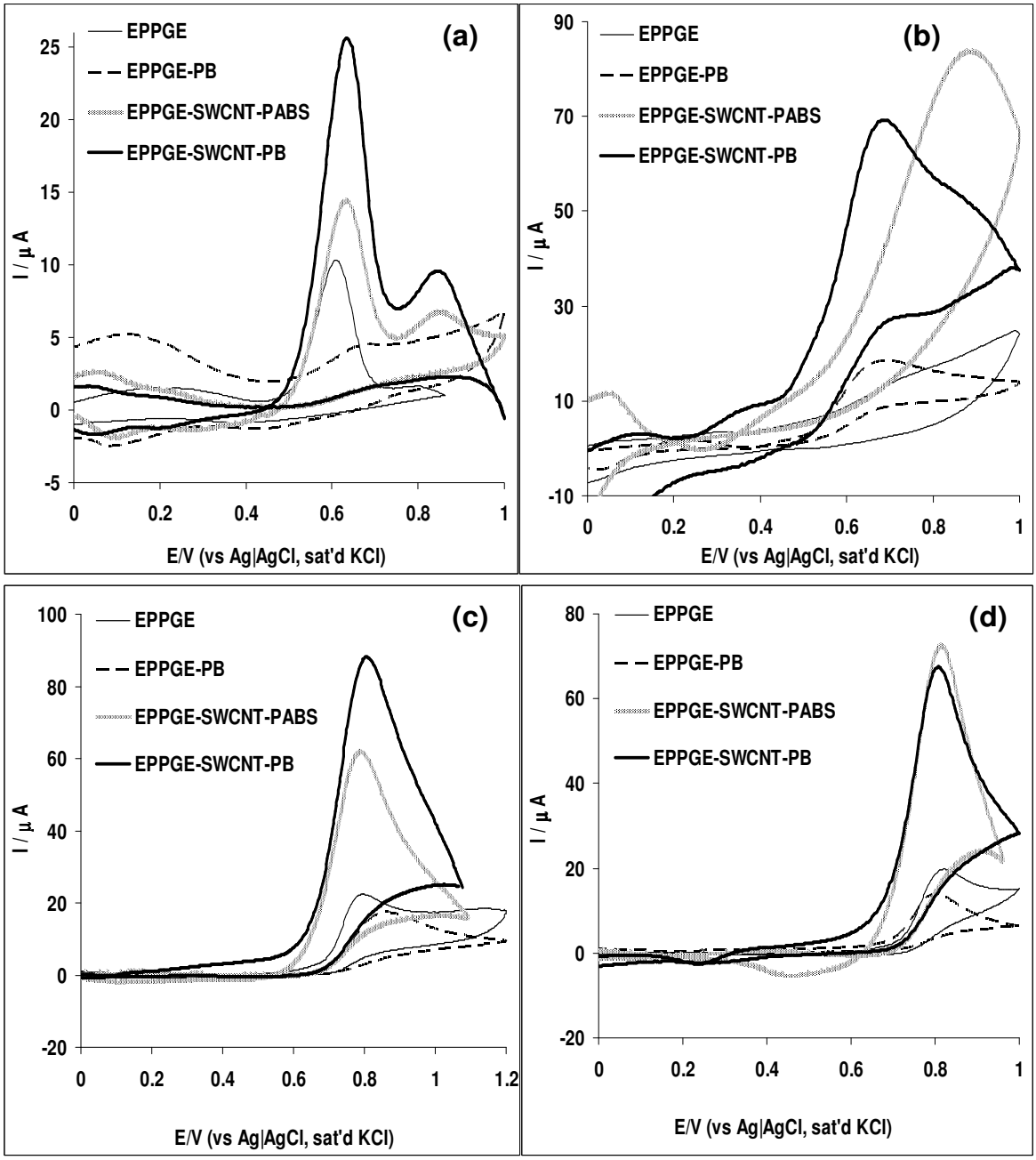

Figure 9.6: Comparative current response (after background current subtraction) of the modified electrodes in (a) 10^{-4} M DEAET in pH 9.4 PBS and (b) 0.1 M Na_2SO_4 solution containing 10^{-3} M hydrazine, (c) 10^{-3} M NO_2^- at pH 7.4 and (d) 10^{-3} M NO at pH 3.0 PBS (Scan rate: 25 mVs^{-1}).

Table 9.1: Electrocatalytic and electroanalytical parameters of the EPPGE-SWCNT-PB towards the detection of DEAET, hydrazine and nitrite. The values in parentheses are values obtained from the linear sweep voltammetry.

Analyte	Electrocatalytic and electroanalytical parameters							
	Electrolyte	E_p/V	Sensitivity/ $\mu A(\mu M)^{-1}$	LCR/μM	LoD/μM	Tafel slope/ $mVdec^{-1}$	$10^{-6}k_{cat}$/ $cm^3mol^{-1}s^{-1}$	ΔG^o/ $kJmol^{-1}$
DEAET	1 M PBS, pH 9.4	0.63	3.05±0.04	28.6 – 37.5	1.43±0.04	273	3.71±0.35	-22.64
Hydrazine	1 M Na_2SO_4	0.68	0.15±0.01	47.6 – 286.0	6.60±0.02	411	7.56±0.68	-25.40
Nitrite	1 M PBS (pH 3.0)	0.80	0.02±0.00	62.5-302.0	6.6±0.50	492	0.64±0.06	-29.53
Nitrite	1 M PBS (pH 7.4)	0.82	0.25±0.03	32.3-286.0	5.4±0.03	279	4.37±0.03	-20.76

The electrocatalytic behaviour of the EPPGE-SWCNT-PB towards the analytes was further interrogated using the impedimetric technique; each study being performed at the peak potential for which the analyte was catalysed. The Nyquist plots obtained from the fitting of the EIS spectra are presented in Figure 9.7a and the data obtained are presented in Table 9.2. Figure 9.7b represents the electrical equivalent circuit used in the fitting. The circuit elements are already defined.

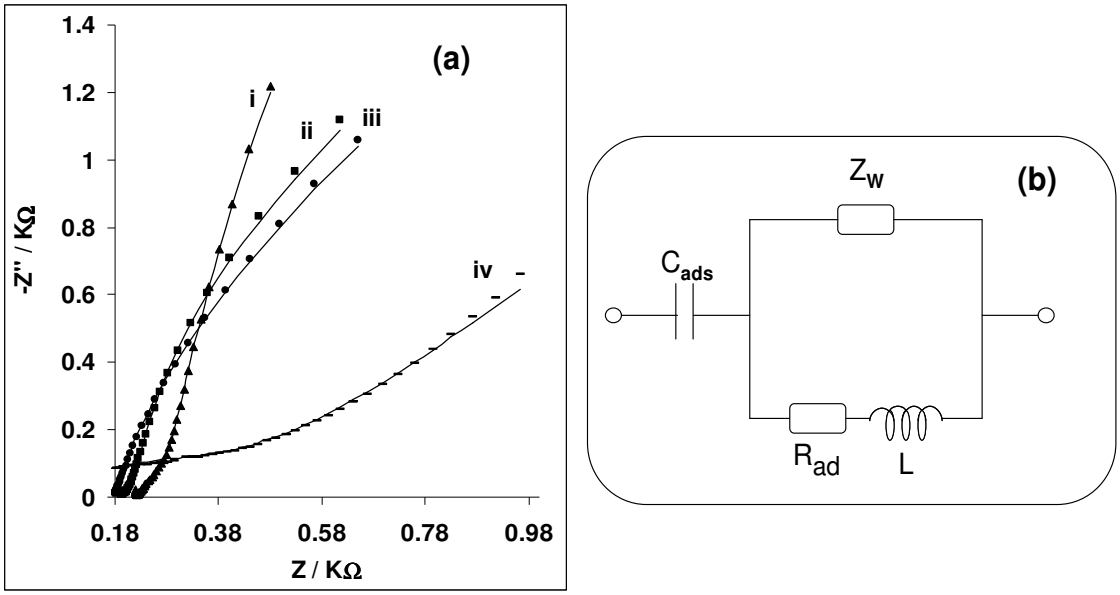

Figure 9.7: (a) Nyquist plots for the EPPGE-SWCNT-PB electrode in (i) 0.1 M pH 9.4 PBS containing 10^{-4} M DEAET, (ii) 0.1 M pH 3.0 PBS containing 10^{-3} M NO, (iii) 0.1 M pH 7.4 PBS containing 10^{-3} M NO_2-, (iv) 0.1 M Na_2SO_4 solution containing 10^{-3} M hydrazine. (b) is the circuit diagram used in the fitting of the impedance data in (a).

The presence of the inductor parameter suggests some adsorption of the reaction intermediate(s) in the overall electrocatalytic processes of these analytes [10,11]. The most

important parameter in Table 9.2 is the R_{ads}, which gave smaller value for the DEAET (20.95 Ωcm^2), an indication that the partial charge transport is faster for the DEAET than for the hydrazine, in the experimental conditions employed. This study has also used EIS measurement to prove adsorption associated with catalysis of the analyte on the PB film which is lack from the other literature reports.

The effect of scan rate (ν) on the electrocatalytic oxidation of the analytes were investigated, exemplified in Figure 8.8 with (a) DEAET. Generally, the oxidation peak potential shifted positively with increasing scan rates for all the analyte studied. The plots of $\log I_p$ vs $\log\nu$ (Figure 9.8b) are linear with slopes values slightly greater than the 0.5 expected fro an ideal diffusion-controlled process, suggesting some involvement of adsorption process [12,13]. Also, the current function plots (I_p/ν vs. ν) obtained for the analytes (Figure 9.8c) gave the characteristic curves confirming the interplay of coupled electrochemical-chemical (EC_{cat}) reactions process at the electrode.

Using the scan rate data and employing the Tafel equation [14], the linear relationships (the peak potential E_p and the $log\upsilon$ (not shown)) confirm the chemical irreversibility of the electrocatalytic oxidation processes of these analytes. The Tafel slopes were 273 mV dec^{-1} (DEAET), 411 mV dec^{-1} (hydrazine), 279 and 492 for nitrite at pH 7.4 and 3.0 respectively. These values are higher than the theoretical 118 mV dec^{-1} for a one-electron process involved in the rate-determining step. Such high Tafel values (leading to small α values, < 0.5) are ascribed to the adsorption of reactants or intermediates on the electrode surfaces and/or reactions occurring within a porous electrode structure [15].

Table 9.2: Impedance data at EPPGE-SWCNT-PB modified electrodes in 10^{-4} M DEAET (in PBS 9.4, at 0.60 V) and 10^{-3} M hydrazine in 0.1 M Na_2SO_4 solution at 0.68 V

Analyte	Electrochemical impedimetric parameters				
	Electrolyte	C_{ads}/μFcm^{-2}	Z_W/μΩcm^2	R_{ads}/ Ωcm^2	L/mHcm^2
DEAET	1 M PBS, pH 9.4	727.0±28.43	1.58±0.02	20.95 ±0.06	0.33 ±0.01
Hydrazine	1 M Na_2SO_4	3040.0±321.94	4.34±0.04	37.20 ±0.14	0.78 ±0.05

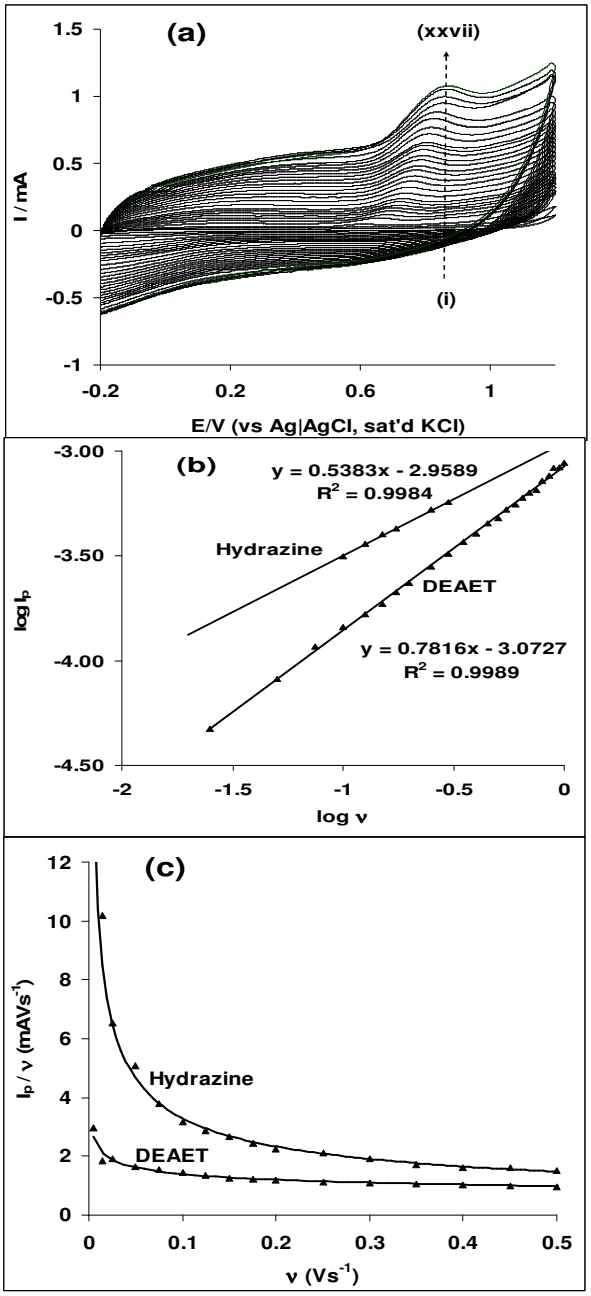

Figure 9.8: Current response of the EPPGE-SWCNT-PB electrode in (a) 0.1 M pH 9.4 PBS containing 10^{-4} M DEAET (scan rates between 25 and 1200 mVs^{-1}, from inner to outer). (b) Plots of E_p vs logν for (I) DEAET and (II) Hydrazine. (c) Current function plots (I_p/ν vs ν).

The catalytic rate constants (k_{cat}) were estimated using chronamperometric technique (at fixed potential of 0.6 V vs Ag|AgCl, sat'd KCl), employing the previous equation 6.6 [16, 17], where I_{cat} and I_{buff} are the currents in the presence and absence of the analyte, C is the bulk concentration and t is the time. From the plots of I_{cat}/I_{buff} vs $t^{1/2}$ at different concentrations of the analytes (exemplified in Figure 9.9a with hydrazine), and a plot of the slopes vs. concentrations of the analytes, the k_{cat} for EPPGE-SWCNT-PB in the analytes were obtained (see Table 9.1). The k_{cat} value of 3.71 x 10^6 $cm^3mol^{-1}s^{-1}$ obtained for DEAET in this study is about 3 times higher than the 1123.59 $M^{-1}s^{-1}$ (i.e., ~ 1.12 x 10^6 $cm^3mol^{-1}s^{-1}$) reported for the SWCNT/cobalt(II)tetraaminophthalocyanine films in DEAET [18]. The k_{cat} value obtained for hydrazine (7.56 x 10^6 $cm^3mol^{-1}s^{-1}$) is about two magnitudes higher than the ~ 2 x10^4 $cm^3mol^{-1}s^{-1}$ for the SWCNT-Ni and SWCNT-Fe films. The difference in the magnitude of k_{cat} could be due to the different electrode modifiers, the different experimental conditions and their degree of interaction with the analytes. Since the CV results suggested some degree of adsorption of these analytes onto the SWCNT-PB films, the adsorptive or stripping linear sweep voltammetry (AdsLSV) technique was employed to analyse the analyte and the Langmuir adsorption theory was used to obtain insights into their degree of adsorption. Each linear sweep voltammogram (LSV) was obtained after gently stirring the analyte for ~15 min in the presence of the electrode. Figure 9.10 is a typical linear sweep voltammetric evolution obtained at different concentrations of the DEAET, hydrazine and nitrite.

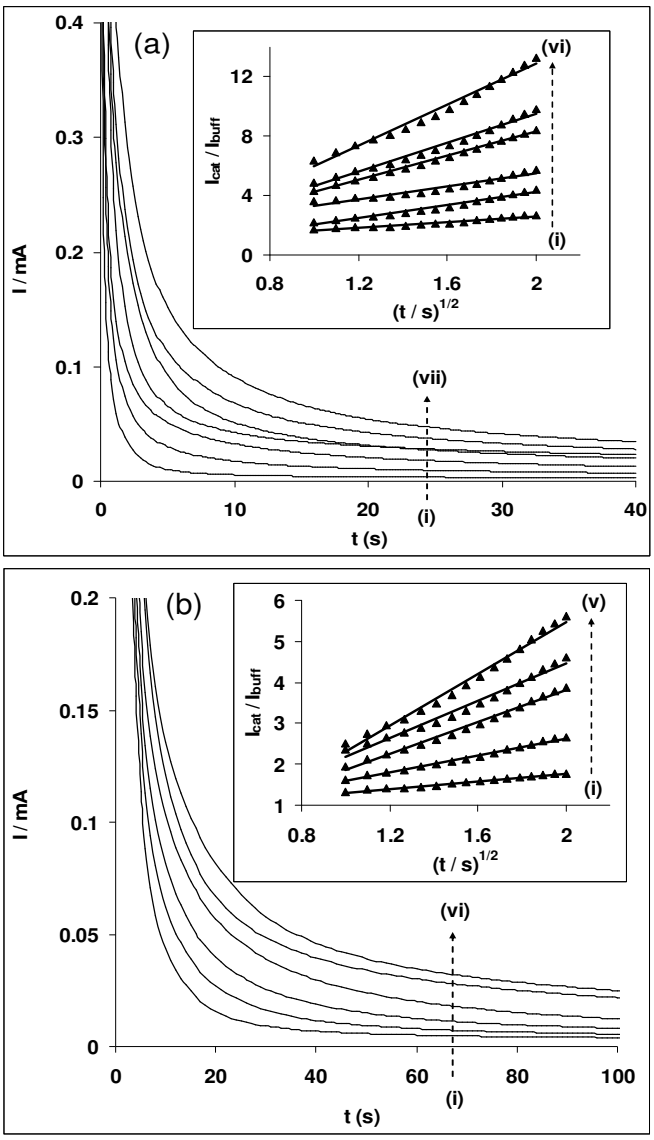

Figure 9.9: Typical chronoamperogram of EPPGE-SWCNT-PB in (a) 0.1 M Na_2SO_4 solution containing different concentrations of hydrazine (0.0, 47.6, 90.9, 130.0, 167.0, 231.0, and 286.0 µM (i to vii)). Inset represents the plots of I_{cat} / I_{buff} vs $t^{1/2}$ obtained from the chronoamperometric evolutions (i-vi correspond to 47.6, 90.9, 130.0, 167.0, 231.0 and 286.0 µM, respectively). (b) pH 9.4 PBS containing different concentrations of DEAET (0.0, 16.7, 23.1, 28.6, 31.0 and 33.3 µM (i to vi)). Inset represents the plots of I_{cat} / I_{buff} vs $t^{1/2}$ obtained from the chronoamperometric evolutions (i-v correspond to 16.7, 23.1, 28.6, 31.0 and 33.3 µM respectively).

The linear sweep voltammograms were analysed using the Langmuir adsorption isotherm theory [19]. From the theory, each plot of the ratio of C/I_{cat} vs C gave straight line (not shown), suggesting an adsorption-controlled process. From the slope and the intercept of the curve obtained, the β value of each analyte was obtained, and then used to estimate the ΔG^o value (Table 9.1). The ΔG^o values are -22.64 kJmol^{-1} (DEAET) and -25.40 kJmol^{-1} (hydrazine) which are in the same fashion as the Tafel slope, suggesting the adsorption behaviour for the different analytes at different experimental/electrolyte conditions.

9.4 Concentration studies and proposed mechanism

Concentration studies were carried out by investigating the response of EPPGE-SWCNT-PB to the different concentrations of the analytes using data from AdsLSV (Figure 9.10). The analytical data, sensitivity, linear range and limit of detection (LoD) obtained from LSV data are summarised in Table 9.1. AdsLSV is the preferred technique in this study due to its reliability over the chronoamperometry. The LoD was calculated based on the relationship (LoD = 3.3δ/s [20]). The detection limits recorded in this work for these analytes are in the same order and lower than several of those reported in the literature. For example, hydrazine has been detected at 8 µM reported on CCE/NiHCF [21], and at 5.3 µM using SWCNT-Ni nanocomposite. The 1.4 µM obtained for DEAET is lower or comparable with some literature reports [18,22,23].

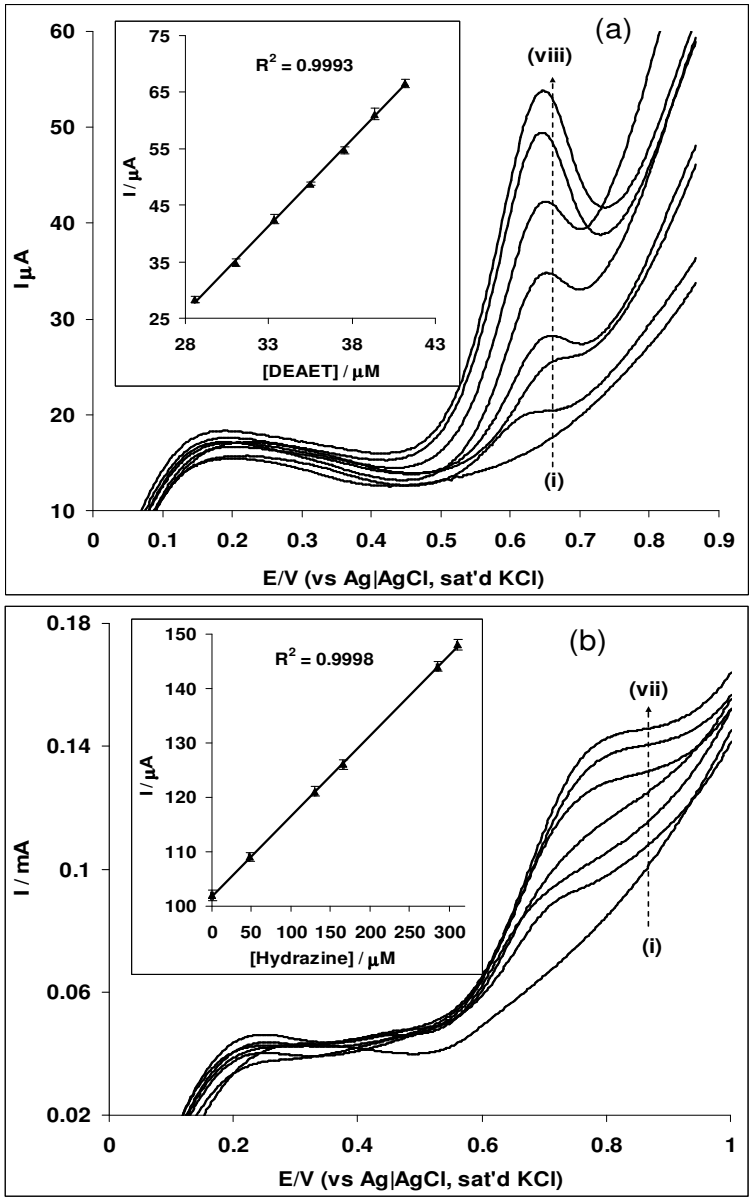

Figure 9.10: Typical linear sweep voltammograms of EPPGE-SWCNT-PB in (a) 0.1 M pH 9.4 PBS containing different concentrations of DEAET (0.0, 20.0, 28.6, 31.0, 33.3, 35.5, 37.5 and 41.2 µM (i) – (viii)). Inset in (a) represents the plot of peak current vs DEAET concentrations. (b) 0.1 M Na_2SO_4 solution containing different concentrations of hydrazine (0.0, 47.6, 90.9, 130.0, 167.0, 200 and 231 mM (i to vii)). Inset in (b) is the plot of peak current vs hydrazine concentrations.

From the results and discussion so far, it may be concluded that the electrocatalytic mechanism is mediated by the PB, summarised as follows:

$$(SWCNT\text{-}PB)_{film} + A_R \longrightarrow (SWCNT\text{-}PB....A_R)_{adduct} \quad (9.1)$$

$$(SWCNT\text{-}PB....A_R)_{adduct} \longrightarrow (SWCNT\text{-}PY)_{film} + A_{Ox} + e^- \quad (9.2)$$

(Rate-determining step)

$$A_{Ox} \longrightarrow \text{Oxidation products} \quad (9.3)$$

$$(SWCNT\text{-}PY)_{film} + ne^- \longrightarrow (SWCNT\text{-}PB)_{film} \quad (9.4)$$

(Regeneration step)

The A_R and A_{OX} represent the reduced and oxidized forms of the analytes, respectively. In general, the mechanism is proposed to involve an initial co-ordination of the reduced form of the analyte with the SWCNT-PB to form an adduct (Equation 9.1). Equation 9.2 is related to the rate-determining step (rds) as discussed in Tafel slope, which involves the oxidation of the PB to its PY form, and the generation of oxidized products such as the thiyl radical ($RS^{\cdot}$) for the DEAET, N_2H_3 for the hydrazine and nitrogen (iv) oxide (NO_2) for nitrite. Other oxidized products (Equation 9.3) include the disulphide products (RSSR) for the DEAET, nitrogen for the hydrazine and nitrate for nitrite. Equation 9.4 represents the subsequent regeneration of the PB catalyst via PY/PW.

In this study, electron-transport and electrocatalytic efficiency of SWCNT/PB nanohybrids towards the oxidation of environmental molecules (DEAET, hydrazine and nitrite) in aqueous media were investigated. The results clearly show that SWCNT/PB nanohybrids represent important electrocatalytic platforms for the sensitive detection of DEAET, hydrazine and nitrite.

References

1. C. C. Rajeev, K-W Jun, C. V. Rode, *Polyhedron* 27 (2008) 933.

2. M. Oku, K. Hirokawa, S. Ikeda, *J. Electron Spectrosc. Relat. Phenom.* 7 (1975) 465.

3. Y-L Hu, J-H Yuan, W. Chen, K. Wang, X-H Xia, *Electrochem. Commun.* 7 (2005) 1252.

4. A. Ernst, O. Makowski, B. Kowalewska, K. Miecznikowski, P. J. Kulesza, *Bioelectrochem.* 71 (2007) 23.

5. J. Wang, *Analytical Electrochemistry*, VCH Publisher Inc., New York, 1994, Chapt. 6, p. 171.

6. A.A. Karyakin, E.E. Karyakina, L. Gorton, *Talanta* (1996) 1597.

7. K. Itaya, N. Shoji, I. Uchida, *J. Am. Chem. Soc.* (1984) 106.

8. N.S. NcIntyre, M.G. Cook, *Anal. Chem.* 47 (1975) 2208.

9. S. Sunohara, K. Nishimura, K. Yahikozawa, M. Ueno, *J. Electroanal. Chem.* 161 (1993) 354.

10. J. Bisquert, H. Randriamahazaka, G. Garcia-Belmonte, *Electrochim. Acta* 51 (2005) 627.

11. M. Jafarian, M. G. Mahjani, H. Heli, F. Gobal, H. Khajehsharifi, M.H. Hamedi, *Electrochim. Acta* 48 (2003) 3423.

12. Y. Shih, J.-M. Zen, A.S. Kumar, P-Y. Chen, *Talanta* 62 (2004) 912.

13. J.-M. Zen, A.S. Kumar, J.-C. Chen, *Anal. Chem.* 73 (2001) 1169.

14. J.A. Harrison, Z.A. Khan, *J. Electroanal. Chem.* 28 (1970) 131.

15. J.N. Soderberg, A.C. Co, A.H.C. Sirk, V.I. Birss, *J. Phys. Chem. B.* 110 (2006) 10401.

16. K.M. Manesh, P. Santosh, A.I. Gopalan, K.P. Lee *Electroanalysis* 18 (2006) 894.

17. Z. Galus, Fundamentals of Electrochemical Analysis, Ellis Horwood Press, New York, 1976, p. 313, Ch. 10.

18. J. Pillay, K.I. Ozoemena, *Electrochim. Acta* 52 (2007) 3630.

19. H.X. Ju, L. Donal, *J. Electroanal. Chem.* 484 (2000) 150.

20. G.D. Christian, *Analytical Chemistry*, 6th ed., John Wiley and Sons, New York, 2004, p. 113.

21. K.C. Pan, C.S. Chuang, S.H. Cheng, Y.O. Su, *J. Electroanal. Chem.* 50 (2001) 160.

22. J. Pillay, K.I. Ozoemena, *Electrochem. Commun.* 9 (2007) 1816.

23. J. Wang, J. Zima, N.S. Lawrence, M.P. Chatrathi, *Anal. Chem*. 76 (2004) 4721.